Eur. Phys. J. A (2013) **49**: 39
DOI 10.1140/epja/i2013-13039-2

THE EUROPEAN PHYSICAL JOURNAL A

Letter

Chiral three-nucleon forces and bound excited states in neutron-rich oxygen isotopes

J.D. Holt[1,2], J. Menéndez[3,4], and A. Schwenk[4,3,a]

[1] Department of Physics and Astronomy, University of Tennessee, Knoxville, TN 37996, USA
[2] Physics Division, Oak Ridge National Laboratory, P.O. Box 2008, Oak Ridge, TN 37831, USA
[3] Institut für Kernphysik, Technische Universität Darmstadt, 64289 Darmstadt, Germany
[4] ExtreMe Matter Institute EMMI, GSI Helmholtzzentrum für Schwerionenforschung GmbH, 64291 Darmstadt, Germany

Received: 11 February 2013
Published online: 22 March 2013

Communicated by U.-G. Meißner

Abstract. We study the spectra of neutron-rich oxygen isotopes based on chiral two- and three-nucleon interactions. First, we benchmark our many-body approach by comparing ground-state energies to coupled-cluster results for the same two-nucleon interaction, with overall good agreement. We then calculate bound excited states in ^{21,22,23}O, focusing on the role of three-nucleon forces, in the standard *sd* shell and an extended $sdf_{7/2}p_{3/2}$ valence space. Chiral three-nucleon forces provide important one- and two-body contributions between valence neutrons. We find that both these contributions and an extended valence space are necessary to reproduce key signatures of novel shell evolution, such as the $N = 14$ magic number and the low-lying states in ^{21}O and ^{23}O, which are too compressed with two-nucleon interactions only. For the extended space calculations, this presents first work based on nuclear forces without adjustments. Future work is needed and open questions are discussed.

Introduction

The oxygen isotopes provide an exciting laboratory, both experimentally and theoretically, to study the structure of extreme neutron-rich nuclei towards and beyond the neutron dripline at ^{24}O [1]. Since ^{24}O is anomalously close to the valley of stability, all bound oxygen isotopes have been explored experimentally [2–10]. The neutron-rich isotopes exhibit surprising new features, such as the closed-shell properties of ^{22}O and ^{24}O, and the corresponding appearance of new magic numbers $N = 14$ and $N = 16$ [11,12]. The spectra with these fingerprints provide a challenge for nuclear theory, and a unique test of nuclear forces and many-body methods for neutron-rich nuclei.

While the chain of oxygen isotopes can be explored by different theoretical methods [12–16], recent studies have focused on ground-state properties relevant for understanding the location of the neutron dripline. In theories based on two-nucleon (NN) forces only, the interactions were found to be too attractive and to predict bound oxygen isotopes to ^{28}O [12]. Coupled-cluster (CC) calculations obtained bound isotopes to ^{25}O with chiral NN forces only, but found the location of the dripline to depend on the resolution scale, implying that higher-body forces need to be considered [13]. The first work including three-nucleon (3N) forces demonstrated that they play a decisive role for the oxygen anomaly and can explain why ^{24}O is the heaviest bound oxygen isotope [12]. Subsequent CC calculations implementing adjusted 3N effects and coupling to the continuum have found similar results [14].

As a result, phenomenological shell-model interactions [17–19] have been developed that are adjusted to correct for these deficiencies. As suggested by Zuker [20], we have shown that these phenomenological adjustments can be largely traced to neglected 3N forces, both for the oxygen ground-state energies [12,21] and in calcium where 3N forces are key for the $N = 28$ magic number [22].

Three-nucleon forces arise because nucleons are finite-mass composite particles that can be excited by interacting with other particles. The pioneering work of Fujita and Miyazawa [23] established the dominance of the single-Delta-excitation mechanism in the long-range part of 3N forces, where one nucleon virtually excites a second nucleon to the $\Delta(1232\,\mathrm{MeV})$ resonance that is then de-excited by interacting with a third nucleon. Additional long- and shorter-range 3N interactions are included naturally in chiral effective field theory (EFT) [24], which provides a systematic expansion for nuclear forces. Similar

[a] e-mail: schwenk@physik.tu-darmstadt.de

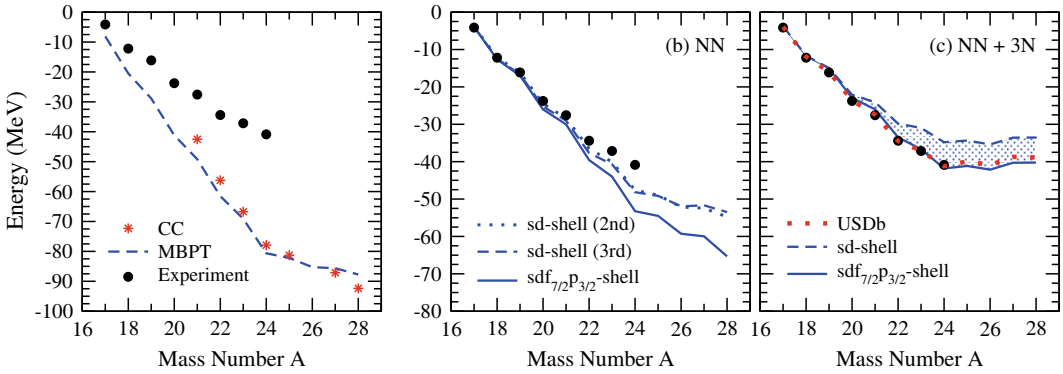

Fig. 1. Ground-state energies of neutron-rich oxygen isotopes relative to ^{16}O, with experimental energies from the AME 2003 atomic mass evaluation [36]. Panel (a) compares results calculated in MBPT to those from CC theory based on the same low-momentum NN interactions. The MBPT results are based on the SPEs obtained in CC theory, for details see text. Panel (b) shows the NN-only MBPT results at 2nd and 3rd order in the *sd* shell, and 3rd order in the $sdf_{7/2}p_{3/2}$ shell, using empirical SPEs. In panel (c), we present the energies obtained at 3rd order from NN and 3N forces, with calculated MBPT SPEs of table 1 that also include 3N contributions, in comparison to the phenomenological USDb model. The band indicates the energy difference between the two valence spaces considered.

to the oxygen and calcium isotopes, chiral 3N forces give repulsive contributions to the neutron and nuclear matter energy [25–28] and to pairing gaps in nuclei [29].

In this paper, we present the first study of the impact of chiral 3N forces on bound excited states in neutron-rich oxygen isotopes. We first discuss the forces and many-body approach used, and benchmark the ground-state energies with CC theory based on the same NN forces. We then calculate the spectra of ^{21,22,23}O in the standard *sd* shell and an extended $sdf_{7/2}p_{3/2}$ valence space, focusing on the role of 3N forces. Our results show that one- and two-body contributions from chiral 3N forces to valence neutrons, included to third order in our many-body formalism, as well as a valence space larger than the standard *sd* shell are important to understand the experimental excited state structures. Extended space calculations present an additional challenge, because potential center-of-mass (cm) admixture must be addressed; we discuss several approaches to clarify this issue.

Interactions among valence neutrons

We calculate the interactions among valence neutrons based on chiral NN and 3N forces following refs. [22, 30]. At the NN level, we first perform a renormalization group (RG) evolution [31,32] of the N^{3}LO NN potential of ref. [33] to a lower resolution scale $\Lambda = 2.0\,\mathrm{fm}^{-1}$. The resulting low-momentum interaction $V_{\mathrm{low}\,k}$ is used to calculate the two-body interactions among valence neutrons to third order in many-body perturbation theory (MBPT), following the formalism of refs. [34,35]. We use a harmonic oscillator basis of 13 major shells with $\hbar\omega = 13.53\,\mathrm{MeV}$, appropriate for the oxygen isotopes. In the MBPT calculations including 3N forces, we also scale the resulting valence-shell interaction and bound single-particle energies (SPEs) by $\hbar\omega \sim A^{-1/3}$. The MBPT results are converged in terms of intermediate-state excitations. In addition to the standard *sd* shell, we also consider an extended $sdf_{7/2}p_{3/2}$ valence space, where the largest changes are due to including the lower-lying $f_{7/2}$ orbital.

To study the validity of the MBPT approach, we have carried out CC calculations for the ground-state energies of the oxygen isotopes, using the same $V_{\mathrm{low}\,k}$ interaction and the same basis space of 13 major shells with $\hbar\omega = 14\,\mathrm{MeV}$. The CC energies are well converged, with a flat $\hbar\omega$ dependence of $\sim 200\,\mathrm{keV}$ change from $\hbar\omega = 14$–$20\,\mathrm{MeV}$. The results are shown in fig. 1 (a) relative to the ground-state energy of ^{16}O. The closed j-subshell systems, ^{16,22,24,28}O, are calculated at the Λ-CCSD(T) level [37] (with small differences from CCSD $\sim 1\,\mathrm{MeV}$). The $A \pm 1$ systems, ^{17,21,23,25,27}O, are obtained with the CC particle-attached/removed equations of motion method at the singles and doubles level (PA/PR-EOM-CCSD) [37].

For the CC comparison, we perform the MBPT calculations in the *sd* shell, where for consistency the SPEs are taken as the PA-EOM-CCSD ($d_{5/2}$, $s_{1/2}$, $d_{3/2}$) energies in ^{17}O. The particle-attached $f_{7/2}$ and $p_{3/2}$ energies are not single particle in character (at this NN level), so the MBPT *sd*-shell comparison provides the cleanest benchmark. In fig. 1 (a), we find that the MBPT energies agree within a few percent with CC theory (the agreement of excitation energies is expected to be even better). This shows that, at this level, MBPT can be comparable to CC theory for $V_{\mathrm{low}\,k}$ interactions, but also highlights the important role of SPEs. Furthermore, comparing with the results shown in figs. 1 (b) or (c), we see that the addition of 3N forces or going to an extended valence space has a greater impact on the ground-state energies than the uncertainty in MBPT in fig. 1 (a).

At the 3N level, we include 3N forces among two valence neutrons and one nucleon in the core. This corresponds to the normal-ordered two-body part of 3N forces, which was found to dominate in CC calculations [38] over residual 3N forces (the latter contributions should be weaker for normal Fermi systems [39]). We take into

Table 1. Empirical and calculated (MBPT) SPEs in MeV.

Orbital	*sd* shell		$sdf_{7/2}p_{3/2}$ shell	
	USDb [17]	MBPT	SDPF-M [18]	MBPT
$d_{5/2}$	−3.93	−3.78	−3.95	−3.46
$s_{1/2}$	−3.21	−2.42	−3.16	−2.20
$d_{3/2}$	2.11	1.45	1.65	1.92
$f_{7/2}$	–	–	3.10	3.71
$p_{3/2}$	–	–	3.10	7.72

account chiral 3N forces at N^{2}LO [40,41] that give rise to repulsive monopole interactions between valence neutrons [12,22]. At N^{2}LO, this includes long-range two-pion–exchange parts c_i (due to Δ and other excitations), plus shorter-range one-pion exchange c_D and 3N contact c_E interactions, with the c_D, c_E couplings fit to the ^{3}H binding energy and the ^{4}He radius for $\Lambda = \Lambda_{3\mathrm{N}} = 2.0\,\mathrm{fm}^{-1}$ [42]. The fit to light nuclei approximately includes effects of the RG evolution in the 3N sector, up to higher-order many-body forces. For all results, these 3N forces, within 5 major oscillator shells, are included fully to third order in MBPT. Future work will be to study the consistent RG evolution of 3N forces and to include N^{3}LO 3N and 4N forces [24].

For the SPEs in ^{17}O, we solve the Dyson equation, consistently including one-body contributions to third order in MBPT in the same space as the two-body interactions. While the convergence in terms of intermediate-state excitations is slower for the one-body energies, the results are still well converged in 13 major shells. In the Dyson equation, we include chiral 3N forces between one valence neutron and two core nucleons, which corresponds to the normal-ordered one-body part of 3N forces. The 3N contributions range between 1.5–3.0 MeV, approximately an order of magnitude larger than typical normal-ordered two-body matrix elements. This is consistent with the normal-ordering hierarchy [38,39]. At each self-consistency iteration, the unperturbed harmonic oscillator spectrum is updated such that the energy of the degenerate valence-space orbitals is set to the centroid, $\sum_j (2j+1)\varepsilon_j/(2j+1)$, of the calculated SPEs of the previous iteration.

Our results for the SPEs in the *sd* and $sdf_{7/2}p_{3/2}$ valence spaces are given in table 1, in comparison with empirical SPEs taken from the USDb [17] and SDPF-M [18] models. With 3N forces included, the resulting SPEs are similar to the empirical values, except that the $p_{3/2}$ orbit is significantly higher. Note that the $f_{7/2}$ orbital is obtained only 2 MeV above the *sd* shell, allowing sizeable contributions from this orbital. It will be important to investigate this issue in improved many-body calculations. Because the higher-lying orbitals are unbound, a necessary future improvement will be to represent these correctly as continuum states. Work in this direction is under development, but CC calculations in this region have found that continuum coupling effectively lowers energies of unbound states only by ~ 300 keV [14].

Following our MBPT strategy, our goal is to work in the largest possible valence space for the diagonalization, which leads to valence spaces involving more than one major harmonic oscillator shell. In such spaces, however, the cm motion does not factorize in general. As in refs. [43, 44], we investigate the possible admixture by adding a cm Hamiltonian, βH_{cm}, with $\beta = 0.5$, to our original Hamiltonian. While the qualitative picture of our results remains, there is some additional compression in the studied spectra as a result (*e.g.*, the 2_1^+ states in ^{22}O and ^{24}O are lowered by 0.9 MeV). This is not unexpected, since the non-zero cm two-body matrix elements are also relevant matrix elements of the MBPT calculation, and making a clear separation between them is therefore difficult. We also find non-negligible $\langle H_{cm} \rangle$ expectation values, 9.1 and 14.8 MeV for the ground states of ^{22}O and ^{24}O, which points to possible cm admixture and/or non-neglible occupancies of the $f_{7/2}$ and $p_{3/2}$ orbitals in the calculations of these neutron-rich nuclei.

However, as discussed in ref. [45] and shown in the context of CC theory [46], β-dependence and $\langle H_{cm} \rangle \neq 0$ do not necessarily imply cm admixture. Given the importance of undertanding this issue, work is in progress in several directions. First, we will apply the singular-value decomposition used in ref. [46] to test cm factorization to extended-space shell-model calculations. In addition, following the MBPT strategy, we will carry out a non-perturbative Okubo-Lee-Suzuki-Okamoto transformation [47–50] into the standard one-major-shell space, where the cm motion factorizes. This treats the MBPT configurations perturbatively, but includes the lower-lying extended-space orbitals non-perturbatively. Finally, we will also apply the in-medium similarity renormalization group (IM-SRG) [51,52] to extended valence spaces, where the cross-shell matrix elements can be driven to small values under the IM-SRG evolution.

Ground-state energies

Although the focus of this work is on excited states, we first discuss results for the ground-state energies in this framework. All calculations based on NN forces are performed with empirical SPEs, and all calculations including 3N forces with the consistently calculated MBPT SPEs of table 1. We take into account many-body correlations by diagonalization in the respective valence spaces using the shell-model code Antoine [53,54]. Figures 1 (b) and (c) show the resulting ground-state energies compared with experiment. With NN forces only, all isotopes out to ^{28}O remain bound because the two-body interactions among valence neutrons are too attractive [12]. Going to the extended $sdf_{7/2}p_{3/2}$ space provides additional attraction, mainly due to the correlations involving the $f_{7/2}$ orbital. To gauge the order-by-order convergence of MBPT, we also show in fig. 1 (b) the ground-state energies to 2nd order. The small difference from 2nd to 3rd order is consistent with the CC agreement and shows that the MBPT calculations can be converged to a good level.

When 3N forces are included in fig. 1 (c), we see their clear repulsive contribution to the ground-state energies, relative to ^{16}O [12]. In both valence spaces, there is significantly less binding compared to the NN-only calculations. The calculated energies in the *sd* shell are underbound with respect to experiment, while in the extended $sdf_{7/2}p_{3/2}$ space, we find very good agreement. Finally, we note that in the $sdf_{7/2}p_{3/2}$ space the ground- and excited-state wave functions contain an admixture of a $2p2h$ intruder configuration. In the NN+3N calculations, the dominant components of the ground-state wave functions, $d_{5/2}$, $f_{7/2}$, and $s_{1/2}$, respectively, change from 3.7, 0.9, 0.2; 4.2, 1.3, 0.3; 4.4, 1.5, 0.9; and 4.4, 1.6, 1.7 from ^{21}O through ^{24}O, showing the expected $s_{1/2}$ filling. In contrast, the corresponding NN-only ground-state wave function occupancies of ^{22}O, 3.6, 0.9, 1.2, reveal a significant $s_{1/2}$ component not present in the NN+3N calculations.

Spectra

Next, we study the properties of bound excited states in the neutron-rich oxygen isotopes ^{21,22,23}O, which have been the subject of recent experimental investigations [4, 5,7,8,10]. While we will not explicitly discuss spectra of the lighter isotopes, we note that in the NN+3N extended-space calculation, the first excited 2^+ (4^+) energies in ^{18}O and ^{20}O are 2.25 MeV (3.90 MeV) and 2.14 MeV (4.99 MeV), respectively, compared with experimental values 1.98 MeV (3.55 MeV) and 1.67 MeV (3.57 MeV). Furthermore, the calculated $E(4^+)/E(2^+)$ ratios of 1.79 and 2.33 for ^{18}O and ^{20}O compare well with the experimental values of 1.73 and 2.14. For each nucleus we discuss and compare with all measured states below the one-neutron separation energy S_n, including for reference the lowest-lying negative-parity state in the odd-mass isotopes. The coupling to the scattering continuum is important for unbound states and as the energies of excited states approach S_n [14,15,55]. Here, we focus on 3N force contributions and note possible continuum effects for the higher-lying states.

^{21}O

The spectrum of ^{21}O in fig. 2 shows clearly the deficiencies of calculations based on NN forces. In a basic *sd*-shell picture, the ground state is interpreted as a one-hole $\frac{5}{2}^+$ state below the ^{22}O closure, while the excited states result from a one-particle excitation to the $s_{1/2}$ orbital coupled to two holes in $d_{5/2}$ with angular momenta 0^+, 2^+, and 4^+ (a $\frac{9}{2}^+$ state is observed above the neutron-decay threshold). These states therefore probe the $d_{5/2}$–$s_{1/2}$ gap. With NN forces only, the calculated spectrum is in very poor agreement with experiment, being too compressed for the low-lying states and too separated for the $\frac{5}{2}^+$ and $\frac{7}{2}^+$ states. Expanding the valence space to the $sdf_{7/2}p_{3/2}$ shell provides only slight improvement for the $\frac{3}{2}^+$ state, but otherwise has little effect.

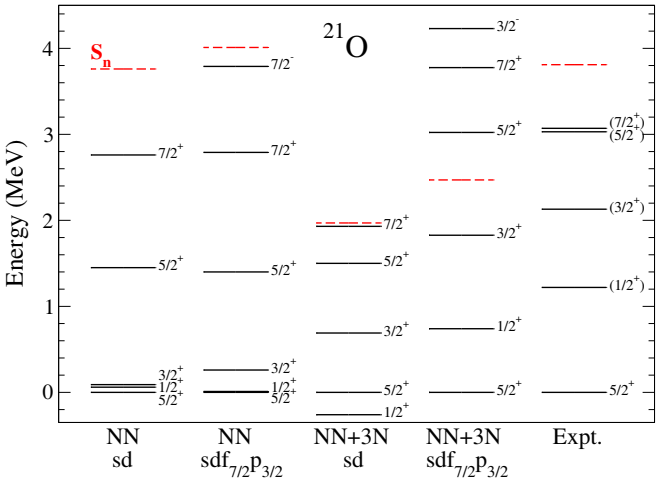

Fig. 2. Excitation energies of bound excited states in ^{21}O compared with experiment [4,10]. The NN-only results are calculated in the *sd* and $sdf_{7/2}p_{3/2}$ shells with empirical SPEs. The NN+3N energies are obtained in the same spaces, but with calculated MBPT SPEs, including 3N contributions to valence two-body interactions and SPEs. The dashed lines give the one-neutron separation energy S_n.

With the inclusion of 3N force contributions, the low-lying states become more spread out, but with an incorrect $\frac{1}{2}^+$ ground state. For the *sd* shell, S_n is well below the experimental value, which reflects the underbound ground-state energies. Our results in the extended $sdf_{7/2}p_{3/2}$ space with 3N forces show significant improvements, although the $\frac{1}{2}^+$ and $\frac{3}{2}^+$ states remain somewhat below the experimental values. Furthermore, due to their presence above the continuum threshold, the $\frac{5}{2}^+_2$ and $\frac{7}{2}^+$ energies may be reduced, bringing them closer to experiment.

^{22}O

The first oxygen isotope exhibiting closed-shell properties for a non-standard magic number, ^{22}O, has its first 2^+ state at almost twice the energy as those in ^{18}O and ^{20}O. In contrast to ^{24}O, whose closed-shell nature can be qualitatively well described in NN-only calculations due to the large separation between the $d_{3/2}$ and $s_{1/2}$ SPEs (see, *e.g.*, ref. [16]), the spectrum of ^{22}O is not well reproduced with NN forces, as shown in fig. 3. In the *sd*-shell, the ground state is predominantly a filled $d_{5/2}$ subshell, while the first excited 2^+ and 3^+ states result from a one-particle $s_{1/2}$ excitation coupled to a $d_{5/2}$ hole. The higher-lying 0^+, 2^+, 4^+ triplet is formed by two excited $s_{1/2}$ particles coupling to two $d_{5/2}$ holes.

With NN forces in the *sd* shell, the first 2^+ state is below experiment, the spacing to the 3^+ state too broad, and the 0^+, 2^+, and 4^+ states are too compressed. Extending the space provides only a slight improvement compared to the experimental spectrum. The addition of 3N forces in the *sd* shell reduces the first 2^+ energy but otherwise improves the level spacings.

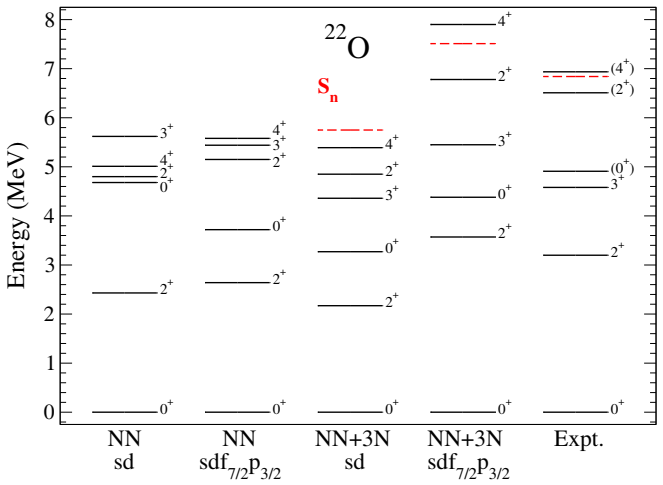

Fig. 3. Excitation energies of bound excited states in ^{22}O compared with experiment [4,5] (labels are as in fig. 2).

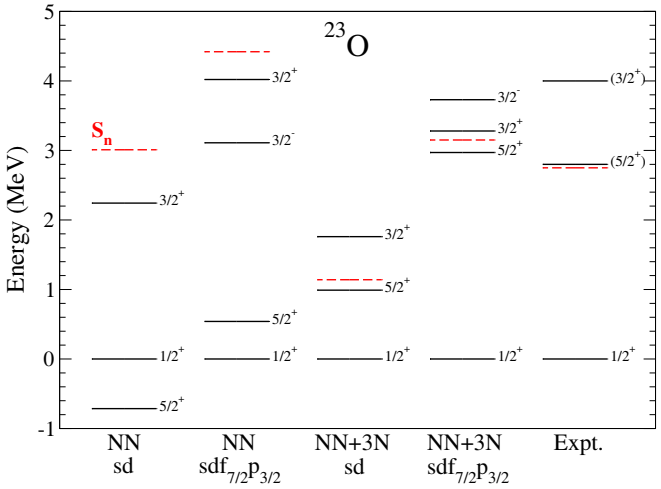

Fig. 4. Excitation energies of bound excited states in ^{23}O compared with experiment [7,8] (labels are as in fig. 2).

It is only when we move to the $sdf_{7/2}p_{3/2}$ space with 3N forces included that we see significant improvement in the spectrum, with the 2_1^+ energy now being approximately twice the 2_1^+ energies of ^{18}O and ^{20}O. Although the 2^+–3^+ splitting is reduced, it is still somewhat large and results in an inversion of the 3^+ and 0^+ states compared with experiment, a feature also seen in all phenomenological USD models. Since the 4^+ energy lies above S_n, some lowering can be expected from continuum effects. Similar to $N = 28$ in calcium [22], we find that both 3N forces and an extended valence space are important for reproducing properties of the $N = 14$ magic number in oxygen.

^{23}O

Occupying a position of particular interest between two doubly magic isotopes, the spectrum of ^{23}O provides a unique test for theory, as it should simultaneously reflect the features of both. The *sd*-shell ^{23}O ground state is dominated by one particle in the $s_{1/2}$ orbit, while the two lowest excited states are expected to be a single particle $\frac{5}{2}^+$ one-hole excitation, indicative of the strength of the ^{22}O shell closure, and a higher-lying single particle $\frac{3}{2}^+$ one-particle excitation, reflecting the strength of the ^{24}O shell closure. Recent experimental measurements of the lowest-lying states in ^{23}O shown in fig. 4 confirm this picture, although no bound excited states are found [7,8]. The $\frac{5}{2}^+$ state lies just above the neutron decay threshold, while the $\frac{3}{2}^+$ state resides well in the continuum, and a complete description cannot ignore these effects.

From fig. 4 we see that the $\frac{5}{2}^+$ state is bound in all calculations. With NN forces in the *sd* shell, the $\frac{5}{2}^+$ state even lies below the $\frac{1}{2}^+$, and the $\frac{3}{2}^+$ is bound, consistent with the expectation of a bound $d_{3/2}$ orbital at ^{24}O without 3N forces [12]. Extending the space to the $sdf_{7/2}p_{3/2}$ orbitals is a clear improvement, and the $\frac{5}{2}^+$ is now 0.54 MeV above the $\frac{1}{2}^+$ ground state. This is similar to the 0.35 MeV excitation energy obtained in CC theory based on a N^{3}LO NN potential only [16].

The repulsive 3N contributions improve the spectrum considerably. We again find the best agreement with experiment in the extended $sdf_{7/2}p_{3/2}$ space, where the enhanced $d_{5/2} - f_{7/2}$ correlations, important for the high 2^+ in ^{22}O, bring the $\frac{5}{2}^+$ energy very close to the experimental value. This shows that 3N forces are essential for the $\frac{5}{2}^+$ state, increasing the excitation energy by ~ 2 MeV compared to the NN-only result. The $\frac{3}{2}^+$ state, however, is significantly lower than experiment lying just beyond the neutron-decay threshold. When continuum coupling is included, this will effectively lower the $d_{3/2}$ orbit [15], pointing to the need to explore uncertainties as well as further improvements in our theoretical approach.

Summary

We have presented the first study of the impact of chiral 3N forces on the spectra of neutron-rich oxygen isotopes. An important next step is to study the theoretical uncertainties of the results, due to the truncation in the chiral EFT expansion, to unceranties in the low-energy couplings in 3N forces, and due to the many-body calculation. Based on the MBPT approach and chiral EFT interactions, we find that the traditional *sd* shell is insufficient, even with 3N forces, to account for key experimental features in the spectra, in particular the $N = 14$ magic number. Going to an extended $sdf_{7/2}p_{3/2}$ valence space, and including NN and 3N contributions to third order in MBPT consistently to the two-body interactions and the one-body SPEs, our results are in good overall agreement with experiment. For the extended space calculations, this presents first work based on nuclear forces without adjustments. Future work is needed, in particular to understand and quantify the potential cm admixture.

We are currently investigating this issue with different approaches. It will also be interesting to study how the physics of the extended valence space may be renormalized into phenomenological *sd*-shell models. In addition, extending our framework to include continuum effects for weakly-bound or unbound states, and for nuclei beyond the driplines, as well as developing non-perturbative approaches to valence shell interactions (see, *e.g.*, refs. [51, 52,56,57]) are important future steps.

We thank G. Hagen, T. Otsuka and T. Suzuki for very useful discussions, and the TU Darmstadt for hospitality. This work was supported in part by US DOE Grant DE-FC02-07ER41457 (UNEDF SciDAC Collaboration), DE-FG02-96ER40963 (UT) and DE-FG02-06ER41407 (JUSTIPEN), by the Helmholtz Alliance Program of the Helmholtz Association, contract HA216/EMMI "Extremes of Density and Temperature: Cosmic Matter in the Laboratory", and the DFG through Grant SFB 634. Computations were performed with an allocation of advanced computing resources on Kraken at the National Institute for Computational Sciences.

References

1. M. Thoennessen, Rep. Prog. Phys. **67**, 1187 (2004).
2. C.R. Hoffman *et al.*, Phys. Rev. Lett. **100**, 152502 (2008).
3. R. Kanungo *et al.*, Phys. Rev. Lett. **102**, 152501 (2009).
4. M. Stanoiu *et al.*, Phys. Rev. C **69**, 034312 (2004).
5. D. Cortina-Gil *et al.*, Phys. Rev. Lett. **93**, 062501 (2004).
6. D. Cortina-Gil *et al.*, Eur. Phys. J. A **25**, 343 (2005).
7. Z. Elekes *et al.*, Phys. Rev. Lett. **98**, 102502 (2007).
8. A. Schiller *et al.*, Phys. Rev. Lett. **99**, 112501 (2007).
9. C.R. Hoffman *et al.*, Phys. Rev. C **83**, 031303(R) (2011).
10. B. Fernández-Domínguez *et al.*, Phys. Rev. C **84**, 011301(R) (2011).
11. T. Otsuka *et al.*, Phys. Rev. Lett. **87**, 082502 (2001).
12. T. Otsuka *et al.*, Phys. Rev. Lett. **105**, 032501 (2010).
13. G. Hagen *et al.*, Phys. Rev. C **80**, 021306(R) (2009).
14. G. Hagen *et al.*, Phys. Rev. Lett. **108**, 242501 (2012).
15. K. Tsukiyama, M. Hjorth-Jensen, G. Hagen, Phys. Rev. C **80**, 051301(R) (2009) K. Tsukiyama, T. Otsuka, R. Fujimoto, arXiv:1001.0729.
16. Ø. Jensen *et al.*, Phys. Rev. C **83**, 021305(R) (2011).
17. B.A. Brown, W.A. Richter, Phys. Rev. C **74**, 034315 (2006).
18. Y. Utsuno *et al.*, Phys. Rev. C **60**, 054315 (1999).
19. F. Nowacki, A. Poves, Phys. Rev. C **79**, 014310 (2009).
20. A.P. Zuker, Phys. Rev. Lett. **90**, 042502 (2003).
21. A. Schwenk, J.D. Holt, AIP Conf. Proc. **1011**, 159 (2008).
22. J.D. Holt *et al.*, J. Phys. G **39**, 085111 (2012).
23. J. Fujita, H. Miyazawa, Prog. Theor. Phys. **17**, 360 (1957).
24. E. Epelbaum, H.-W. Hammer, U.-G. Meißner, Rev. Mod. Phys. **81**, 1773 (2009).
25. S.K. Bogner *et al.*, Nucl. Phys. A **763**, 59 (2005).
26. K. Hebeler *et al.*, Phys. Rev. C **83**, 031301(R) (2011)).
27. J.W. Holt, N. Kaiser, W. Weise, Phys. Rev. C **81**, 024002 (2010).
28. K. Hebeler, A. Schwenk, Phys. Rev. C **82**, 014314 (2010).
29. T. Lesinski *et al.*, J. Phys. G **39**, 015108 (2012).
30. A.T. Gallant *et al.*, Phys. Rev. Lett. **109**, 032506 (2012).
31. S.K. Bogner *et al.*, Nucl. Phys. A **784**, 79 (2007).
32. S.K. Bogner *et al.*, Prog. Part. Nucl. Phys. **65**, 94 (2010).
33. D.R. Entem, R. Machleidt, Phys. Rev. C **68**, 041001(R) (2003).
34. T.T.S. Kuo, E. Osnes, Lect. Notes Phys. **364**, 1 (1990).
35. M. Hjorth-Jensen, T.T.S. Kuo, E. Osnes, Phys. Rep. **261**, 125 (1995).
36. G. Audi, A.H. Wapstra, C. Thibault, Nucl. Phys. A **729**, 337 (2003).
37. G. Hagen *et al.*, Phys. Rev. C **82**, 034330 (2010).
38. G. Hagen *et al.*, Phys. Rev. C **76**, 034302 (2007).
39. B. Friman, A. Schwenk, in *From Nuclei to Stars: Festschrift in Honor of Gerald E. Brown*, edited by S. Lee (World Scientific, 2011) arXiv:1101.4858.
40. U. van Kolck, Phys. Rev. C **49**, 2932 (1994).
41. E. Epelbaum *et al.*, Phys. Rev. C **66**, 064001 (2002).
42. S.K. Bogner *et al.*, arXiv:0903.3366.
43. D.J. Dean *et al.*, Phys. Rev. C **59**, 2474 (1999).
44. E. Caurier, J. Menéndez, F. Nowacki, A. Poves, Phys. Rev. C **75**, 054317 (2007).
45. J.B. McGrory, B.H. Wildenthal, Phys. Lett. B **60**, 5 (1975).
46. G. Hagen, T. Papenbrock, D.J. Dean, Phys. Rev. Lett. **103**, 062503 (2009).
47. S. Okubo, Prog. Theor. Phys. **12**, 603 (1954).
48. S.Y. Lee, K. Suzuki, Phys. Lett. B **91**, 173 (1980).
49. K. Suzuki, S.Y. Lee, Prog. Theor. Phys. **64**, 2091 (1980).
50. K. Suzuki, R. Okamoto, Prog. Theor. Phys. **70**, 439 (1983).
51. K. Tsukiyama, S.K. Bogner, A. Schwenk, Phys. Rev. Lett. **106**, 222502 (2011).
52. K. Tsukiyama, S.K. Bogner, A. Schwenk, Phys. Rev. C **85**, 061304 (2012).
53. E. Caurier, F. Nowacki, Acta. Phys. Pol. **30**, 705 (1999).
54. E. Caurier, G. Martínez-Pinedo, F. Nowacki, A. Poves, A.P. Zuker, Rev. Mod. Phys. **77**, 427 (2005).
55. N. Michel *et al.*, J. Phys. G **37**, 064042 (2010).
56. A.F. Lisetskiy *et al.*, Phys. Rev. C **78**, 044302 (2008).
57. G.R. Jansen *et al.*, Phys. Rev. C **83**, 054306 (2011).